Visible Raman-Shifted Fiber Lasers for Biophotonic Applications

Timothy H. Runcorn, Frederik G. Görlitz, Robert T. Murray, and Edmund J. R. Kelleher

(Invited Paper)

***Abstract*—The efficient nonlinear conversion of Yb-doped fiber laser systems using a combination of stimulated Raman scattering and second-harmonic generation is an effective method for developing sources for biophotonic applications in the yellow–green spectral region. In this paper, we review recent progress in the development of these sources, compare the relative benefits of differing source architectures, and demonstrate stimulated emission depletion microscopy using an exemplar source.**

***Index Terms*—Fiber lasers, stimulated Raman scattering (SRS), second-harmonic generation (SHG), biophotonics.**

I. Introduction

PULSED laser sources in the yellow-green (550–600 nm) spectral region are required for a variety of cutting-edge biophotonic imaging applications such as optical-resolution photoacoustic microscopy (OR-PAM) [1] and stimulated emission depletion (STED) microscopy [2]. OR-PAM uses the detection of ultrasound waves, generated by the thermoelastic expansion of molecules caused by the absorption of focused pulsed laser light, to form a volumetric image [3]. This non-invasive hybrid imaging modality enables *in vivo* label-free functional imaging based on optical absorption contrast with micrometer lateral resolution [4]. STED microscopy enables imaging with a better resolution than is allowed by the Abbe diffraction limit by utilizing two lasers—an excitation beam and a depletion beam—to spatially manipulate the molecular states of the specimen. The wavelength of the depletion beam is located in the red-shifted tail of the emission spectrum of the fluorescent label to deplete the excited state by the process of stimulated emission.

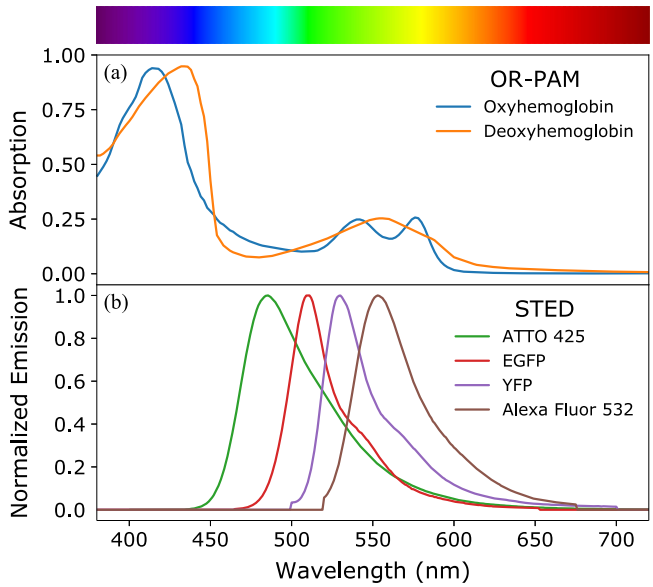

Fig. 1. (a) Absorption spectra of oxyhemoglobin and deoxyhemoglobin in 1 mm of blood. (b) Normalized emission spectra of fluorophores used with a STED depletion beam in the yellow-green spectra region. Color bar above of the visible light spectrum.

Both OR-PAM and STED microscopy achieve the best performance using laser sources with tens to hundreds of nanojoules of pulse energy, nanosecond-duration pulses and near diffraction-limited beam quality [4], [5]. These parameters are readily obtainable in the wavelength range 515–550 nm from compact and efficient frequency-doubled Yb:fiber master oscillator power amplifier (MOPA) systems. Beyond this wavelength range, however, lie the differential absorption features of oxyhemoglobin and deoxyhemoglobin [Fig. 1(a)], used for functional OR-PAM [6] and the emission peaks of several key fluorescent labels used in STED microscopy [Fig. 1(b)]. To access these absorption and emission features via second-harmonic generation (SHG) thus requires operating Yb:fiber MOPA systems at wavelengths longer than 1100 nm. Unfortunately, the larger emission cross-section of Yb-doped fibers at shorter wavelengths makes this difficult to achieve in high-gain MOPA systems, and so alternative sources of gain need to be considered.

Manuscript received August 7, 2017; revised October 28, 2017; accepted October 31, 2017. Date of publication November 3, 2017; date of current version December 1, 2017. This work was supported in part by the Engineering and Physical Sciences Research Council under Grants EP/N009452/1 and EP/K503733/1, in part by the European Office of Aerospace Research and Development under Grant FA9550-17-1-0194, and in part by the Royal Academy of Engineering ("NextGenLasers" [RF/115]). *(Corresponding author: Timothy H. Runcorn.)*

T. H. Runcorn and R. T. Murray are with the Femtosecond Optics Group, Department of Physics, Imperial College London, London SW7 2BW, U.K. (e-mail: timothy.runcorn07@imperial.ac.uk; robert.murray10@imperial.ac.uk).

F. G. Görlitz is with the Photonics Group, Department of Physics, Imperial College London, London SW7 2BW, U.K. (e-mail: f.gorlitz14@imperial.ac.uk).

E. J. R. Kelleher is with the Femtosecond Optics Group, Department of Physics, Imperial College London, London SW7 2BW, U.K., and also with the Quantum Matter Institute, University of British Columbia, Vancouver BC V6T 1Z4, Canada (e-mail: edmund.kelleher08@imperial.ac.uk).

Color versions of one or more of the figures in this paper are available online at http://ieeexplore.ieee.org.

Digital Object Identifier 10.1109/JSTQE.2017.2770101

Stimulated Raman scattering (SRS) offers an efficient means to frequency downshift radiation that is guided within the transparency window of an optical fiber (0.3–2.4 μm for silica fibers). SRS in optical fibers can, therefore, be used in conjunction with SHG to access the yellow-green spectral region using Yb:fiber laser systems. This technique has been widely applied to develop continuous-wave (CW) yellow-green sources for applications such as laser guide star [7], [8] and STED microscopy [9]. For STED microscopy, pulsed laser sources are preferred, particularly for live cell imaging, since a better resolution improvement can be obtained with significantly less average power in comparison to CW depletion beam sources. In photoacoustic microscopy, high pulse energies are advantageous to maximize the signal to noise ratio whilst complying with laser safety standards. In this paper, we review current state-of-the-art pulsed yellow-green Raman-shifted Yb:fiber MOPA systems, discuss the relative merits of the different approaches used, and demonstrate the applicability of these sources for STED microscopy.

A. *Stimulated Raman Scattering in Optical Fibers*

The Raman effect describes the small fraction ($\sim 10^{-6}$) of light that is inelastically scattered by a molecular medium. In the scattering event, the incident optical photon excites the molecule into a virtual energy state, from which it relaxes to an excited vibrational state. This results in the emission of a lower frequency photon (Stokes wave) and the creation of an optical phonon corresponding to the quantized energy difference between the vibrational states. If the molecule is already in the excited vibrational state, the scattering event results in the emission of a higher frequency photon (anti-Stokes wave) and the annihilation of an optical phonon. Boltzmann statistics, however, predict that the majority of molecules will be in their ground state at room temperature making this process less likely to occur.

The spontaneous Raman scattering process can be stimulated by the presence of the Stokes wave, which grows exponentially with a gain coefficient proportional to the pump intensity and the imaginary part of the third-order nonlinear susceptibility tensor [10], [11]. This SRS process enables efficient energy transfer from the pump to the Stokes wave, providing gain to the spontaneously scattered Stokes light or photons injected at the Stokes-shifted frequency. The magnitude of the Raman gain coefficient is dependent on the frequency separation between the pump and Stokes waves, and is governed by the vibrational resonances of the molecules involved. In optical fibers, the amorphous nature of the glass matrix causes inhomogenous broadening of the resonances, resulting in a broadband Raman gain that extends over 40 THz. The dominant peak in the Raman gain curve of pure silica-core optical fibers occurs at a frequency downshift of 13.2 THz (blue line Fig. 2), and it is an order of magnitude larger when the pump and Stokes waves are co-polarized in comparison to the orthogonally polarized case.

Optical fibers are an ideal platform for harnessing SRS as an efficient nonlinear conversion technique due to the high optical intensity that is maintained in the core over interaction lengths that can be up to several kilometers. The Raman gain is sufficiently high when using kilowatt-level pump peak-powers, typical of pulsed Yb:fiber MOPA systems, that >90% of the pump power can be transferred to the amplified spontaneous Raman scattering at the first Stokes shift within a few meters of fiber [12]. Increasing the pump peak-power further leads to the formation and amplification of spontaneous Raman scattering at the second Stokes shift, depleting the power at the first Stokes shift. This cascaded SRS can transfer power to many higher-order Stokes shifts, but successive Stokes orders typically have lower spectral extinction and a larger spectral bandwidth due to competing nonlinear effects such as self- and cross-phase modulation (SPM and XPM) and four-wave mixing (FWM) [13]–[15].

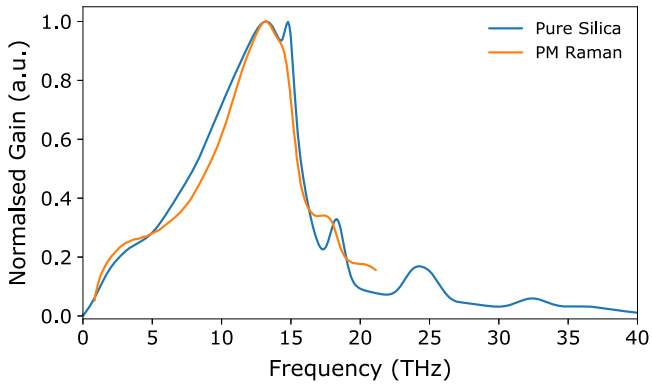

Fig. 2. Calculated Raman gain curve for a pure silica-core optical fiber, based on the multiple vibrational mode model [21] and specified Raman gain curve of OFS PM Raman Fiber.

B. *Second-Harmonic Generation*

Second-harmonic generation (SHG) describes the parametric second-order nonlinear effect where two pump photons are annihilated and a single photon of twice the frequency is created, and thus is interchangeably described as frequency-doubling [16], [17]. It is one of the most commercially significant nonlinear optical processes, primarily used to convert the output of near infrared (NIR) lasers into the ultraviolet (UV) and visible spectral regions. In contrast to SRS, which is automatically phase-matched by the medium, efficient SHG requires phase-matching, such that momentum of the three interacting waves is conserved. This can be achieved by using crystals where the birefringence cancels the chromatic dispersion or by periodically reversing the domains of a suitable crystal, such that the addition of the wave vector corresponding to the domain inversion grating results in quasi phase-matching (QPM).

The two main considerations when choosing a crystal for SHG performed in conjunction with SRS are the effective nonlinear coefficient and the spectral acceptance bandwidth of the crystal. To achieve high SHG conversion efficiency, the effective nonlinear coefficient dictates the amount of pump peak-power required and the spectral acceptance bandwidth determines the maximum pump spectral bandwidth that can be tolerated. Of the birefringent crystals, lithium triborate (LBO) is an attractive choice for accessing the yellow-green spectral region since non-critical phase-matching (NCPM) can be implemented for SHG

TABLE I
VISIBLE RAMAN-SHIFTED YB:FIBER MOPA SYSTEMS

Scheme	Seed	SHG Crystal	Wavelength (nm)	Average Power (W)	Pulse Duration (ns)	Repetition Rate (MHz)	Pulse Energy (nJ)	Ref.
SHG → Raman	None	–	585	0.04	∼2	1	40	[26]
SHG → Raman	None	–	600	0.05	∼2	1	50	[26]
SHG → Raman	None	–	616	0.07	∼2	1	70	[26]
SHG → Raman	None	–	558	0.020	∼1*	0.04	490	[6]
SHG → Raman	None	–	580	0.013	∼1*	0.04	335	[6]
SHG → Raman	None	–	590	0.015	∼1*	0.04	365	[6]
SHG → Raman	None	LBO	560	1.0	∼1.3	1	1000	[27]
SHG → Raman	None	LBO	575	0.9	∼1.3	1	900	[27]
Raman → SHG	None	LBO	589	36	∼2*	25	1440	[28]
Raman → SHG	None	LBO	615	27	∼2*	25	1080	[28]
Raman → SHG	FBG	PPLN	585	1.0	∼1	20	50	[29]
Raman → SHG	FBG	PPLN	600	0.5	∼1	20	25	[29]
Raman → SHG	FBG	PPLN	616	1.0	∼1	20	50	[29]
Raman → SHG	DFB	PPLN	560	0.45	0.15	47.5	10	[30]
Raman → SHG	DFB	PPLT	560	1.53	2.7	2	765	[31]
Raman → SHG	DFB	PPLN	589	1.13	1.9	6	188	[32]
Yb-Raman → SHG	RFL	LBO	589	1.01	∼0.1*	32	32	[33]
Yb-Raman → SHG	RFL	LBO	565	22.5	∼3.8*	2	11250	[34]

*Fundamental pulse duration.

between 1030–1240 nm by varying the crystal temperature over the range 194–9 °C, respectively. NCPM has the advantages over critical phase-matching of no spatial walk-off and a wider angular acceptance bandwidth. The spectral acceptance bandwidth of LBO is relatively broad at 3.8 nm·cm for SHG of 1064 nm pump light at a crystal temperature of 149 °C for NCPM [18]. The primary disadvantage of LBO is its relatively modest effective nonlinear coefficient (∼0.85 pm/V [19]), thus relatively high (>10 kW) pump peak-power is required to achieve high SHG conversion efficiency [20].

Significantly higher nonlinear coefficients can be obtained using periodically poled (PP) ferroelectric crystals such as lithium niobate (PPLN), lithium tantalate (PPLT) and potassium titanyl phosphate (PPKTP). NCPM is achieved using these crystals via QPM by the periodic reversal of the crystal domains on a micrometer length scale. Lithium niobate has the highest nonlinear coefficient of the ferroelectric crystals, with PPLN devices typically having an effective nonlinear coefficient of ∼16 pm/V [22]. The main drawback of PPLN, however, is its high susceptibility to photorefractive damage (PRD), which leads to catastrophic damage if the generated green light intensity is too high [23]. Doping PPLN crystals with 5 mol.% magnesium oxide (MgO) and operating at temperatures >150°C increases the PRD threshold to around 10 MW/cm^2 [24]. PPLT and PPKTP have significantly higher photochromic damage thresholds, at the expense of a reduced nonlinearity, with typical devices having an effective nonlinear coefficient of ∼9 pm/V [22].

When selecting a SHG crystal, the higher effective nonlinear coefficient that can be obtained via QPM using PP ferroelectric crystals in comparison to LBO has to be balanced against a vastly reduced spectral acceptance bandwidth. As an example, the spectral acceptance bandwidth for a PPLT crystal with a 7.8 μm pitch grating for SHG of 1064 nm is 0.24 nm·cm, more than an order of magnitude smaller than for LBO [25]. This poses a severe limitation on the spectral bandwidth of the fundamental, which needs to be significantly smaller than the spectral acceptance bandwidth to achieve a high SHG conversion efficiency.

II. YELLOW-GREEN YB:FIBER MOPA CONVERSION SCHEMES

A number of architectures have been effectively demonstrated that convert pulsed Yb:fiber MOPA systems into the yellow-green spectral region, using a combination of Raman-shifting and SHG. Table I summarizes the output parameters of illustrative sources from the literature of these different schemes. Broadly, three distinct approaches have emerged. Arguably the most conceptually straightforward and widely used scheme involves using cascaded SRS in a passive (non-rare-earth-doped) fiber to frequency downshift the output of a frequency-doubled Yb:fiber MOPA system [Fig. 3(a)]. The main drawbacks of this approach relate to the need to couple high power green light into the passive fiber. To avoid this, the Yb:fiber MOPA system can be Raman-shifted before the SHG stage. This Raman-shifting can either be performed in a passive fiber spliced to the Yb:fiber MOPA output [Fig. 3(b)] or within the active (rare-earth-doped) fiber of the power amplifier stage [Fig. 3(c)]. In the proceeding sections we discuss in detail the relative benefits of these three approaches.

A. SHG Followed by Raman-Shifting

The greatest benefit of performing the frequency-doubling first is the spectral flexibility of the Raman-shifted wavelength it affords. By simply varying the peak-power coupled into the Raman-shifting fiber, the Stokes shift that contains the majority of the spectral power can be selected. Using a pump wavelength of 532 nm, the first five Stokes shifts corresponding to a peak frequency downshift of 13.2 THz occur at 545 nm, 558 nm, 572 nm, 587 nm and 603 nm. Thus it is possible to cover the entire yellow-green spectral region using a passive fiber to Raman-shift the output of a frequency-doubled Yb:fiber MOPA system.

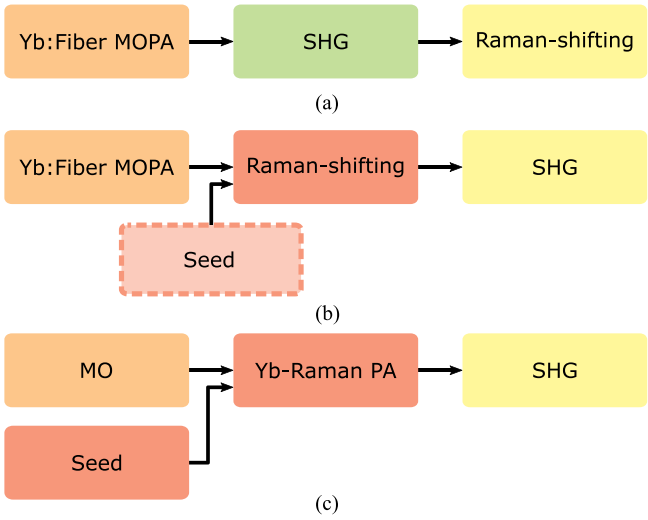

Fig. 3. Demonstrated schemes for nonlinear conversion of Yb:fiber MOPA systems into the yellow-green spectral region. (a) Raman-shifting of a frequency-doubled Yb:fiber MOPA system. (b) Frequency-doubling a Raman-shifted Yb:fiber MOPA system with optional seed at the corresponding Stokes shift. (c) Frequency-doubling a combined Yb-Raman power amplifier (PA) with pulses from a master oscillator (MO) in the Yb:fiber gain band.

This technique has been successfully applied in several demonstrations, three of which that are applicable to OR-PAM and STED microscopy are listed in Table I. Rankin *et al.* pumped a 100 m length of single-mode polarization-maintaining (PM) fiber using a frequency-doubled Yb:fiber MOPA system operating at 530 nm, with a pulse duration of 2 ns at a repetition rate of 1 MHz [26]. They achieved pulses energies of 40 nJ, 50 nJ and 70 nJ at the Stokes shifts of 585 nm, 600 nm, 616 nm and applied this to STED microscopy of yellow-green fluorescent beads and PtK2 cells with vimentin fibers tagged with Chromeo 488. In their paper, they noted that the transmission of the Raman-shifting fiber decreased by 40% shortly after coupling in the pump light, which was caused by photodarkening.

Photodarkening is a severe issue when using standard step-index single mode fibers to guide high peak-power green light for several reasons [35]. Firstly, color center formation—the process that causes photodarkening—occurs at a much higher rate for green light in contrast to near-infrared light due to the proximity of two-photon absorption (TPA) features of molecular bond sites. Secondly, the mode-field diameter (MFD) of standard single-mode fibers for green light is typically around 4 μm, resulting in very high optical intensities in the core which further accelerates photodarkening. Finally, standard step-index fibers typically have a slightly germanium-doped core, which makes them far more susceptible to photodarkening since the breaking of the Ge-Si bond by TPA results in color center formation. The issue of photodarkening can largely be mitigated by using visible single-mode fibers with a pure silica core. Other photo-induced damage mechanisms, however, make the long-term reliability of such fibers questionable for the generation of high peak-power visible radiation.

Hajireza *et al.* used a 40 kHz frequency-doubled Yb:fiber laser with a pulse duration of 1 ns to pump a 3 m length of single-mode PM fiber with a pure silica core [6]. They achieved pulse energies of 490 nJ, 335 nJ and 365 nJ at the Stokes shifts of 558 nm, 580 nm and 590 nm, which were used for *in vivo* OR-PAM of a capillary network in a mouse ear. The increased pulse energy obtained over the results in [26] was largely due to the shorter fiber length used, which requires a proportionally higher pump peak-power to access the same Raman Stokes shift.

The scaling of the Raman-shifted pulse energy (whilst maintaining nanosecond pulse durations) by shortening the Raman-shifting fiber length is limited to a few hundred nanojoules by spectral broadening due to competing nonlinear effects. Pumping shorter fiber lengths with higher peak-powers increases the relative impact of SPM, XPM and FWM. This effect was demonstrated in the results presented by Xu *et al.* [27], where scaling the pulse energy of the 575 nm Stokes shift to the microjoule-level resulted in a 3 dB spectral bandwidth of 12.3 nm, when using standard single-mode fiber. This broad spectral bandwidth leads to poor spectral extinction between the individual Stokes shifts and results in power loss in applications where the output is spectrally filtered.

To scale the pulse energy beyond this limit, Xu *et al.* pumped a 15 m length of large mode-area (LMA) photonic crystal fiber (PCF) using a frequency-doubled Yb:fiber MOPA system with pulse duration of 1.3 ns at a repetition rate of 1 MHz. The endlessly single-mode pure silica fiber used had a specified mode-field diameter of 8 μm, leading to a mode-field area that was approximately four times greater than standard single-mode fibers for the visible. This enabled the authors to achieve a pulse energy of 1.0 μJ and 0.9 μJ at the Stokes shifts of 560 nm and 575 nm with spectral bandwidths equivalent to using the same length of standard single-mode fiber, but with nearly double the pulse energy.

B. Raman-Shifting Followed by SHG

Unseeded Raman amplification: The main benefit of performing the Raman-shifting before the frequency-doubling is that the Raman-shifting fiber can be fusion spliced directly to the Yb:fiber MOPA, removing the need to free-space couple green light into an optical fiber. This has a threefold advantage: firstly, it removes the need to couple into a small-core fiber, which is extremely sensitive to thermal drift and pointing stability. Secondly, the loss (typically ~40%) associated with the coupling efficiency is eliminated, increasing the overall source efficiency. Finally, there are no reliability issues with passive optical fibers in the near-infrared associated with photodarkening or other photo-induced damage.

For a pump wavelength of 1064 nm, the first three Stokes shifts corresponding to a peak frequency downshift of 13 THz occur around 1120 nm, 1178 nm and 1240 nm, which can be frequency-doubled to 560 nm, 589 nm and 620 nm, respectively. Therefore, frequency-doubled Raman-shifted Yb:fiber MOPA systems can also cover the yellow-green spectrum, but wavelength tuning is much more difficult to implement as it requires either mechanical or thermal adjustment of the SHG crystal to maintain phase-matching. The main issue of frequency-doubling a Raman-shifted Yb:fiber MOPA system is

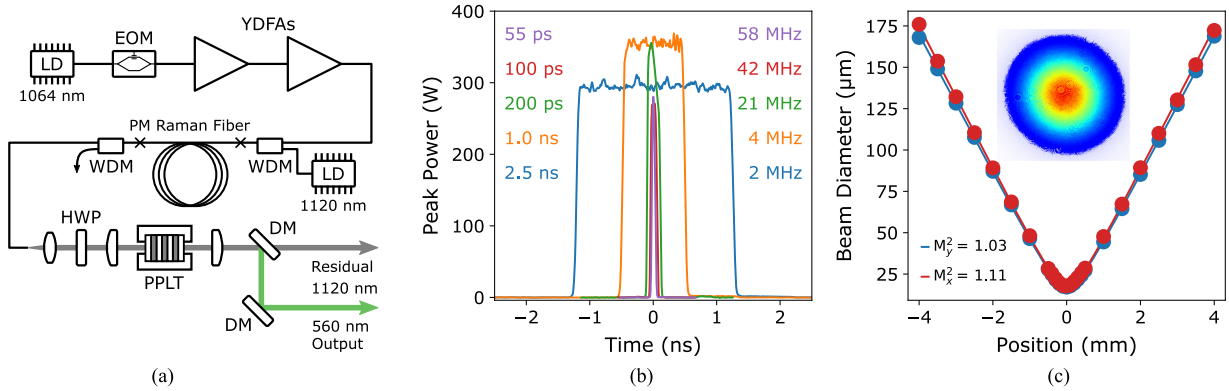

Fig. 4. Example 560 nm source, employing a Raman-shifting followed by SHG approach [31]. (a) Schematic of the system. LD, laser diode; EOM, electro-optic modulator; YDFAs, ytterbium-doped fiber amplifiers; WDM, wavelength division multiplexer; HWP, half wave plate; PPLT, periodically poled lithium tantalate; DM, dichroic mirror. (b) Duration-tunable 560 nm pulses. (c) Beam quality measurement with CCD camera image of the collimated beam (inset).

the large spectral bandwidth of the generated amplified spontaneous Raman scattering, due to the broad Raman gain bandwidth in silica optical fibers (Fig. 2). This can limit the SHG conversion efficiency due to the finite spectral acceptance bandwidths of frequency-doubling crystals.

The impact of the finite spectral acceptance bandwidth was demonstrated by Avdokhin *et al.* [28], where a Yb:fiber MOPA system was Raman-shifted to 1178 nm and 1230 nm and then frequency-doubled using LBO. The Yb:fiber MOPA system operated at 1064 nm with a pulse duration of approximately 2 ns at a repetition rate of 25 MHz. A maximum SHG conversion efficiency of 35% was obtained for generating 589 nm light, decreasing to 30% at maximum fundamental power, corresponding to a pulse energy of 1.4 μJ. The decrease in SHG conversion efficiency, in spite of the increased peak-power of the fundamental, was caused by spectral broadening of the 1178 nm Raman-shifted radiation. For generating 615 nm light, an SHG conversion of 25% was obtained, resulting in a pulse energy of 1.1 μJ. The broader spectral acceptance bandwidth of LBO for SHG of 1230 nm was countered by the increased spectral bandwidth of the Raman-shifted radiation, which is typically observed as the Stokes order is increased.

The relatively low SHG conversion efficiency obtained for the Raman-shifted systems in [28] is in part due to the modest nonlinear coefficient of LBO. As discussed in Section I-B, significantly higher effective nonlinear coefficients can be obtained using PP crystals, at the expense of a vastly reduced spectral acceptance bandwidth. The low power spectral density of the amplified spontaneous Raman scattering, however, would lead to extremely poor SHG conversion efficiencies if PP crystals were utilized.

Seeded Raman amplification: To overcome the power spectral density issue, a narrow linewidth seed can be injected at the Raman Stokes shift that subsequently undergoes Raman amplification by a pulsed pump. The virtual nature of the energy levels involved in Raman amplification result in the Raman gain only being available in the window of the pump pulses. Therefore, the temporal properties of the Raman amplifier are mainly determined by the pump pulses, whereas, the spectral characteristics are predominantly determined by seed. This enables pulsed Yb:fiber MOPA systems to be frequency downshifted with a spectral bandwidth suitable for efficient SHG using PP crystals.

Keaton *et al.* used two pairs of fiber Bragg gratings (FBG) that reflected a narrow bandwidth at the second and third Raman shifts (1170 nm and 1232 nm) to seed the SRS process [29]. The linear cavity, formed by a passive fiber length and the two matched FBGs, was pumped by a Yb:fiber MOPA system with a 1.2 ns pulse duration and 20 MHz repetition rate that was frequency downshifted to 1111 nm by unseeded SRS. The round-trip time of the linear cavity was six times the period of the pump pulses, and thus the narrow bandwidth reflected Stokes pulses were synchronously pumped with six pulses circulating in the cavity. The output of the synchronously pumped Raman laser was frequency-doubled using a 10 mm long PPLN crystal, which had three QPM grating periods for sum-frequency generation (SFG) of the two Stokes shifts (1170 nm and 1230 nm) and SHG of each individual shift. A pulse energy of 50 nJ was achieved at 585 nm and 616 nm via SHG and 20 nJ was obtained at 600 nm via SFG with a pulse duration of $\sim$1 ns at the pump repetition rate of 20 MHz.

The main drawback of synchronously pumped Raman lasers is that the pump repetition rate needs to be precisely tuned to the Raman cavity length, thereby precluding repetition rate adjustment and pulse-duration tunability. To overcome this limitation, in our recent works we used narrow linewidth continuous-wave (CW) signals to seed Raman amplifiers that were pulse-pumped using Yb:fiber MOPA systems [30]–[32].

In [31], an electro-optic modulator (EOM) was used in conjunction with a pulsed laser diode as the master oscillator of a Yb:fiber MOPA system, which pulse-pumped a Raman amplifier seeded by a CW signal at 1120 nm from a distributed feedback (DFB) laser diode [Fig. 4(a)]. The output of the Raman amplifier was frequency-doubled using a 20 mm long PPLT crystal with SHG conversion efficiencies exceeding 50%. The duration of the generated 560 nm pulses could be continuously tuned over the range 55 ps–2.7 ns with the repetition rate adjusted over the range 58–2 MHz to maintain an approximately

constant pump peak-power. An average power of >0.9 W was achieved across the entire tuning range, resulting in a peak-power of ~300 W for the 560 nm pulses [Fig. 4(b)]. A maximum pulse energy of 765 nJ was obtained at a repetition rate of 2 MHz with a pulse duration of 2.7 ns. The beam quality of the collimated frequency-doubled output was near diffraction limited, with a measured $M^2 \leq 1.11$ [Fig. 4(c)].

In [32], we extended the CW seeded, pulsed-pumped Raman amplifier concept to the second Stokes shift at 1179 nm by using a cascaded Raman amplifier architecture. The 1120 nm output of a CW-seeded Raman amplifier (pulse-pumped by a Yb:fiber MOPA system) was used to pulse-pump a second Raman amplifier stage that was seeded by a CW signal at 1179 nm from a DFB laser diode. The output of the cascaded Raman amplifier was frequency-doubled in a 20 mm long PPLN crystal. A maximum 589 nm pulse energy of 188 nJ was achieved at a repetition rate of 6 MHz with a pulse duration of 1.9 ns.

The benefit of using a discreet, pulse-pumped Raman amplifier architecture is that the Raman gain of the amplifier can be optimized to suit the peak-power of the Yb:fiber MOPA pump system. This comes at the expense of the insertion loss of the wavelength division multiplexers (WDM) and splice loss between fibers with mismatching MFDs. In addition, the inevitable extra passive fiber between the Yb:fiber MOPA and the Raman amplifier restricts the maximum peak-power due to deleterious SRS, limiting the power-scaling potential.

Seeded and combined Yb-Raman amplification: To overcome the drawbacks of discreet Raman amplifiers, an alternative approach is to introduce the CW signal at the Stokes shift before the final power amplifier stage in the Yb:fiber MOPA system [Fig. 3(c)]. By choosing the amplifier fiber characteristics (length, MFD, pump absorption, etc.) and the peak-power of pulses correctly, efficient Raman conversion can occur in the amplifier itself. The output of these combined Yb-Raman amplifiers can then be directly frequency-doubled into the the yellow-green spectral region with no additional losses or nonlinear spectral broadening.

This technique was first demonstrated by Dupriez *et al.*, where a cascaded Raman fiber laser (RFL) was used to provide a CW signal at 1178 nm that was combined with 140 ps pulses at 1060 nm and amplified in a 23 m long single-mode Yb-doped fiber [33]. The output of the amplifier was frequency-doubled using a 15 mm long LBO crystal, generating a maximum 589 nm pulse energy of 32 nJ at a repetition rate of 32 MHz. The SHG conversion efficiency was very low (4%) in this demonstration due to nonlinear effects (SPM, XPM and FWM) broadening the 1178 nm signal linewidth to a 3 dB spectral bandwidth of 8 nm.

In more recent work, Rowen *et al.* combined a CW RFL operating at 1130 nm with 3.8 ns pulses at 1080 nm in an LMA Yb-doped fiber in a fully fiber integrated system [34]. The output of the amplifier was frequency-doubled using a 30 mm long LBO crystal with a maximum SHG conversion efficiency of 35%. Using a 915 nm pump power of 85 W, a maximum 565 nm pulse energy of 11.3 μJ was obtained at a repetition rate of 2 MHz with a corresponding pump to yellow-green light conversion efficiency of 26%.

This result represents the highest pulse energy obtained from a visible Raman-shifted pulsed Yb:fiber MOPA system, highlighting the power scalability of the combined Yb-Raman amplifier concept. In addition, the pump to yellow-green light conversion efficiency is almost certainly the highest of the systems reviewed here, but this cannot be confirmed due to a lack of reported efficiency values. It is worth noting, however, that this high pump conversion occurred at average power levels that would not be suitable for biophotonic applications, primarily due to the high peak-power required to obtain efficient SHG in LBO.

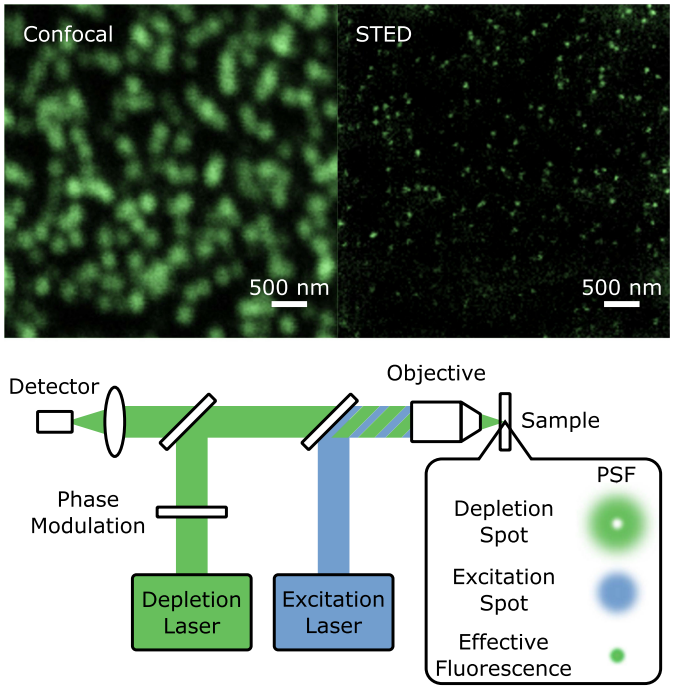

Fig. 5. Schematic of a STED microscopy setup and images of yellow-green fluorescent beads taken using a 560 nm fiber laser depletion beam source with confocal image for comparison.

C. Application to STED Microscopy

STED microscopy enables imaging in greater detail than is allowed by the diffraction limit of traditional confocal laser scanning fluorescence microscopy, through the addition of a second laser source to spatially manipulate the molecular states of the fluorophores employed. To achieve this, a phase pattern is applied to the depletion beam such that its point spread function (PSF) at the focus of the microscope objective lens has a central intensity minimum (preferably zero), typically a "doughnut" shape (Fig. 5). The depletion beam suppresses the fluorescence, generated by the spatially overlapped Gaussian excitation beam, in the periphery of the spot by the process of stimulated emission. As the pulse fluence of the depletion beam is increased, the saturation of the fluorescence suppression causes the central area of unaffected fluorescence to shrink, resulting in an effective fluorescence PSF that can be smaller than the Abbe diffraction limit. For effective fluorescence suppression, the depletion beam should have a wavelength in the long-wavelength tail of the targeted fluorophore emission spectrum, to avoid re-excitation whilst having an appreciable stimulated emission cross section.

The green fluorescent protein (GFP) is one of the most widely used fluorophores in fluorescence microscopy because the GFP gene can be introduced and expressed in a wide variety of biological species. This allows the intrinsic labeling of specific cells in living organisms, enabling *in vivo* and live cell imaging by negating the need for extrinsic fluorophores, which are often phototoxic. The maximum of the emission spectrum of enhanced GFP (EGFP) occurs at 510 nm [red line Fig. 1(b)], so for effective fluorescence supression in STED microscopy, the depletion beam wavelength should be in the range $\sim$540–600 nm [36]. For live cell STED microscopy, a pulsed depletion beam is strongly preferred over CW lasers since a significant resolution improvement can be obtained with average powers below the photodamage limit. Fluorescence suppression of GFP is most efficient with a pulse duration in the range 0.1–2 ns, with longer pulses being beneficial for increasing the pulse energy whilst avoiding photobleaching due to excessive peak-power [5].

The source detailed in Fig. 4 has been incorporated as the depletion beam in a STED microscopy setup designed for imaging with GFP, for which it is ideally suited. To test the effectiveness of the source for fluorescence depletion, 46 nm diameter polystyrene beads with a yellow-green fluorescent label (Thermo Fisher Scientific) were imaged using the setup. A resolution of $<$50 nm was achieved using a STED depletion average power (before the 100$\times$ oil immersion objective) of 12 mW at a repetition rate of 10 MHz, significantly better than the $\sim$240 nm resolution of the confocal image with the depletion beam off (Fig. 5). The resolution was mainly limited by the Nyquist criteria imposed by the 25 nm pixel size. A spatial light modulator was used to impart the phase pattern on the depletion beam in the setup, which enables the correction of aberrations and enhancement of the axial resolution [37]. The sub-diffraction-limited effective fluorescence PSF was detected after dichroic filters using a hybrid photomultiplier tube, allowing time gating to be applied to the STED image. The 485 nm pulsed laser diode used for the excitation beam was triggered off the STED depletion laser with an electronically adjustable time delay. This demonstration highlights the suitability of visible Raman-shifted fiber lasers as compact and robust depletion beam sources for STED microscopy.

III. Conclusion

In conclusion, it has been shown that SRS can be used in conjunction with SHG to efficiently convert the output of pulsed Yb:fiber MOPA systems into the yellow-green spectral region. The nanosecond duration pulses obtained at wavelengths across the 550–620 nm spectral region with hundreds of nanojoules of pulse energy by the systems reviewed in this paper are ideally suited to applications in biophotonics, such as OR-PAM and STED microscopy. It was discussed that the order in which the SRS and SHG are performed has a significant impact on the output parameters achievable and the practical aspects of the laser sources. Performing the SHG first has the major advantage of flexible output wavelength that can be selected from the cascaded SRS orders simply by adjusting the coupled pump peak-power. The issue of coupling high intensity green light into the Raman-shifting fiber, however, raises questions about the long-term reliability and the robustness of these sources. Performing the SRS before SHG eliminates these practical issues but sacrifices the possibility of fast wavelength tuning, which is particularly desirable for functional OR-PAM. Of the different Raman-shifting combined with SHG conversion architectures that have been reported, systems where the Raman-shifting is performed within the power amplifier of the Yb:fiber MOPA have demonstrated the highest pulse energies and potentially the greatest overall conversion efficiency. The utility of a visible Raman-shifted fiber laser for biophotonic imaging techniques was demonstrated by imaging poylstyrene beads with a resolution $<$50 nm using a STED microscopy setup. We predict the increasing deployment of these sources in biomedical imaging applications owing to their unique combination of output parameters in a compact and robust format.

Acknowledgment

The authors would like to thank J. R. Taylor, C. Dunsby, and P. M. W. French for engaging discussions and the generous use of their experimental apparatus for the results presented herein.

References

[1] K. Maslov, H. F. Zhang, S. Hu, and L. V. Wang, "Optical-resolution photoacoustic microscopy for in vivo imaging of single capillaries," *Opt. Lett.*, vol. 33, pp. 929–931, May 2008.

[2] S. W. Hell and J. Wichmann, "Breaking the diffraction resolution limit by stimulated emission: Stimulated-emission-depletion fluorescence microscopy," *Opt. Lett.*, vol. 19, pp. 780–782, Jun. 1994.

[3] P. Beard, "Biomedical photoacoustic imaging," *Interface Focus*, pp. 602–631, Jun. 2011.

[4] Y. Wang *et al.*, "Fiber-laser-based photoacoustic microscopy and melanoma cell detection," *J. Biomed. Opt.*, vol. 16, Jan. 2011, Art. no. 0110141.

[5] D. Wildanger, E. Rittweger, L. Kastrup, and S. W. Hell, "STED microscopy with a supercontinuum laser source," *Opt. Express*, vol. 16, pp. 9614–9621, Jun. 2008.

[6] P. Hajireza, A. Forbrich, and R. Zemp, "In-vivo functional optical-resolution photoacoustic microscopy with stimulated Raman scattering fiber-laser source," *Biomed. Opt. Express*, vol. 5, pp. 539–546, Feb. 2014.

[7] A. Friedenauer *et al.*, "RFA-based 589-nm guide star lasers for ESO VLT: A paradigm shift in performance, operational simplicity, reliability, and maintenance," *Proc. SPIE*, vol. 8447, Sep. 2012, Art. no. 84470F.

[8] L. Zhang, H. Jiang, S. Cui, J. Hu, and Y. Feng, "Versatile Raman fiber laser for sodium laser guide star," *Laser Photon. Rev.*, vol. 8, pp. 889–895, Jul. 2014.

[9] G. Moneron *et al.*, "Fast STED microscopy with continuous wave fiber lasers," *Opt. Express*, vol. 18, pp. 1302–1309, Jan. 2010.

[10] E. J. Woodbury and W. K. Ng, "Ruby laser operation in near IR," in *Proc. Inst. Radio Engineers*, Nov. 1962, vol. 50, p. 2367.

[11] A. Penzkofer, A. Laubereau, and W. Kaiser, "High intensity Raman interactions," *Prog. Quant. Electron.*, vol. 6, pp. 55–140, 1979.

[12] C. Lin, L. Cohen, R. Stolen, G. Tasker, and W. French, "Near-infrared sources in the 1–1.3 μm region by efficient stimulated Raman emission in glass fibers," *Opt. Commun.*, vol. 20, no. 3, pp. 426–428, Mar. 1977.

[13] G. Pei-Juan, N. Cao-Jiang, Y. Tian-Long, and S. Hai-Zheng, "Stimulated Raman scattering up to 10 orders in an optical fiber," *Appl. Phys.*, vol. 24, pp. 303–306, Apr. 1981.

[14] G. Rosman, "High-order comb spectrum from stimulated Raman scattering in a silica-core fibre," *Opt. Quantum Electron.*, vol. 14, pp. 92–93, Jan. 1982.

[15] R. H. Stolen, C. Lee, and R. K. Jain, "Development of the stimulated Raman spectrum in single-mode silica fibers," *J. Opt. Soc. Amer. B*, vol. 1, pp. 652–657, Aug. 1984.

[16] P. A. Franken, A. E. Hill, C. W. Peters, and G. Weinreich, "Generation of optical harmonics," *Phys. Rev. Lett.*, vol. 7, pp. 118–119, Aug. 1961.

[17] J. A. Armstrong, N. Bloembergen, J. Ducuing, and P. S. Pershan, "Interactions between light waves in a nonlinear dielectric," *Phys. Rev.*, vol. 127, pp. 1918–1939, Sep. 1962.
[18] K. Kato, "Temperature-tuned 90° phase-matching properties of LiB_3 O_5," *IEEE J. Quantum Electron.*, vol. 30, no. 12, pp. 2950–2952, Dec. 1994.
[19] D. Roberts, "Simplified characterization of uniaxial and biaxial nonlinear optical crystals: A plea for standardization of nomenclature and conventions," *IEEE J. Quantum Electron.*, vol. 28, no. 10, pp. 2057–2074, Oct. 1992.
[20] A. V. Babushkin, D. V. Gapontsev, N. S. Platonov, and V. P. Gapontsev, "Pulsed fiber laser with 30 W output power at 532 nm," *Proc. SPIE*, vol. 6102, Feb. 2006, Art. no. 61021E.
[21] D. Hollenbeck and C. D. Cantrell, "Multiple-vibrational-mode model for fiber-optic Raman gain spectrum and response function," *J. Opt. Soc. Amer. B*, vol. 19, pp. 2886–2892, Dec. 2002.
[22] I. Shoji, T. Kondo, A. Kitamoto, M. Shirane, and R. Ito, "Absolute scale of second-order nonlinear-optical coefficients," *J. Opt. Soc. Amer. B*, vol. 14, pp. 2268–2294, Sep. 1997.
[23] A. Ashkin *et al.*, "Optically-induced refractive index inhomogeneities in $LiNbO_3$ and $LiTaO_3$," *Appl. Phys. Lett.*, vol. 9, pp. 72–74, Jul. 1966.
[24] F. Kienle *et al.*, "Green-pumped, picosecond MgO:PPLN optical parametric oscillator," *J. Opt. Soc. Amer. B*, vol. 29, pp. 144–152, Jan. 2012.
[25] I. Dolev *et al.*, "Linear and nonlinear optical properties of MgO:$LiTaO_3$," *Appl. Phys. B*, vol. 96, pp. 423–432, Aug. 2009.
[26] B. R. Rankin and S. W. Hell, "STED microscopy with a MHz pulsed stimulated-Raman-scattering source," *Opt. Express*, vol. 17, pp. 15 679–15 684, Aug. 2009.
[27] L. Xu, S. Alam, Q. Kang, D. P. Shepherd, and D. J. Richardson, "Raman-shifted wavelength-selectable pulsed fiber laser with high repetition rate and high pulse energy in the visible," *Opt. Express*, vol. 25, pp. 351–356, Jan. 2017.
[28] A. Avdokhin *et al.*, "High average power quasi-CW single-mode green and UV fiber lasers," *Proc. SPIE*, vol. 9347, Feb. 2015, Art. no. 934704.
[29] G. L. Keaton, M. W. Byer, M. J. Leonardo, M. Martinez, and K. Monro, "Multi-color laser source for STED microscopy," *Proc. SPIE*, vol. 7905, Feb. 2011, Art. no. 79050W.
[30] T. H. Runcorn *et al.*, "Fiber-integrated frequency-doubling of a picosecond Raman laser to 560 nm," *Opt. Express*, vol. 23, pp. 15 728–15 733, Jun. 2015.
[31] T. H. Runcorn, R. T. Murray, E. J. R. Kelleher, S. V. Popov, and J. R. Taylor, "Duration-tunable picosecond source at 560 nm with watt-level average power," *Opt. Lett.*, vol. 40, pp. 3085–3088, Jul. 2015.
[32] T. Runcorn, R. T. Murray, E. J. Kelleher, and J. R. Taylor, "Watt-level nanosecond 589 nm source by SHG of a cascaded Raman amplifier," in *Proc. Adv. Solid State Lasers*, Oct. 2016, Paper ATh1A.3.
[33] P. Dupriez *et al.*, "1 W average power at 589 nm from a frequency doubled pulsed Raman fiber MOPA system," *Proc. SPIE*, vol. 6102, Feb. 2006, Art. no. 61021G.
[34] E. E. Rowen, G. Vashdi, J. Lasri, and E. Inbar, "A scalable high-power yellow laser source based on frequency doubling of a combined Yb-Raman fiber amplifier," *Proc. SPIE*, vol. 8961, Mar. 2014, Art. no. 89611P.
[35] L. J. Poyntz-Wright, M. E. Fermann, and P. S. J. Russell, "Nonlinear transmission and color-center dynamics in germanosilicate fibers at 420–540 nm," *Opt. Lett.*, vol. 13, pp. 1023–1025, Nov. 1988.
[36] B. R. Rankin *et al.*, "Nanoscopy in a living multicellular organism expressing GFP," *Biophys. J.*, vol. 100, pp. L63–L65, Jun. 2011.
[37] M. O. Lenz *et al.*, "3D stimulated emission depletion microscopy with programmable aberration correction," *J. Biophoton.*, vol. 7, pp. 29–36, Jan. 2014.

Timothy H. Runcorn received the M.Sci. degree in physics, the M.Res. degree in photonics, and the Ph.D. degree from Imperial College London, London, U.K., in 2011, 2012, and 2016, respectively. Since 2016, he has been a Research Associate with the Femtosecond Optics Group, Imperial College London. He is currently an Engineering and Physical Sciences Research Council Doctoral Prize Fellow. He has authored/co-authored more than 20 articles in peer-reviewed journals and conference proceedings. His research interests include fiber lasers and amplifiers, nonlinear optics, and the development of laser sources for biophotonic applications.

Frederik G. Görlitz received the B.Sc. and M.Sc. degrees in physics from Karl Ruprechts University, Heidelberg, Germany, in 2011 and 2013, respectively. He is currently working toward the Ph.D. degree in physics at Imperial College London, London, U.K. His research interest includes the development and application of superresolution microscopy in combination with fluorescence lifetime imaging, working toward high-content analysis with a functional readout via FLIM-FRET.

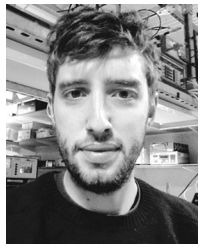

Robert T. Murray received the M.Phys. degree from the University of Manchester, Manchester, U.K., in 2010, and the M.Res. and Ph.D. degrees in photonics from Imperial College London, London, U.K., in 2011 and 2015, respectively. He is currently a Research Associate in the Femtosecond Optics Group, Imperial College London. He has authored/coauthored more than 20 papers in peer-reviewed journals and conference proceedings. His research interests include high-power fiber amplifier and laser systems, nonlinear frequency conversion techniques and materials, and mid-infrared coherent sources.

Edmund J. R. Kelleher was born in Norwich, England, in 1986. He received the B.Eng. degree in electronic engineering from the University of Warwick, Coventry, U.K., in 2007, the M.Sc. degree in photonics and optoelectronic devices from the University of St. Andrews, St. Andrews, U.K., and Heriot-Watt University, Edinburgh, U.K., in 2008, and the Ph.D. degree in physics from Imperial College London, London, U.K., in 2012.

From 2012 to 2013, he was a Research Associate at Imperial College London, supported by the Engineering and Physical Sciences Research Council. In 2014, he became a Royal Academy of Engineering Research Fellow, the position he currently holds within the Department of Physics, Imperial College London. In 2017, he joined the Quantum Matter Institute, University of British Columbia, Vancouver, BC, Canada, as a Visiting Research Scientist. He has published more than 50 peer-reviewed journal articles, and has served on the programme committees of several international conferences. His research interests include the interface of fundamental and applied nonlinear optics, with themes including soliton dynamics, parametric processes, supercontinuum generation, and optical frequency combs. Exploiting such processes, his work targets the development of high-energy, ultrafast pulse sources covering regions of the UV, visible, near-IR, and mid-IR for applications ranging from superresolution optical microscopy to electron spectroscopy. He also has a strong interest in the optical characterization and application of low-dimensional nanomaterials for the development of advanced photonic devices, and the application of machine learning and AI in optics.

Dr. Kelleher was the recipient of the Paterson Medal by the Institute of Physics in 2015.